A Manifold Alignment Approach for Hyperspectral Image Visualization with Natural Color

Danping Liao, Yuntao Qian, *Member, IEEE*, Jun Zhou, *Senior Member, IEEE* and Yuan Yan Tang, *Fellow, IEEE*

***Abstract*—Trichromatic visualization of hundreds of bands in a hyperspectral image has been an active research topic. The visualized image shall convey as much information as possible from the original data and facilitate easy image interpretation. However, most existing methods display hyperspectral images in false color, which contradicts with user experience and expectation. In this paper, we propose a new framework for visualizing hyperspectral image with natural color by fusion of a hyperspectral image and a high-resolution color image via manifold alignment. Manifold alignment projects several data sets to a shared embedding space where the matching points between them are pairwise aligned. The embedding space bridges the gap between the high dimensional spectral space of the hyperspectral image and the RGB space of the color image, making it possible to transfer natural color and spatial information in the color image to the hyperspectral image. In this way, a visualized image with natural color distribution and fine spatial details can be generated. Another advantage of the proposed method is its flexible data setting for various scenarios. As our approach only needs to search a limited number of matching pixel pairs that present the same object, the hyperspectral image and the color image can be captured from the same or semantically similar sites. Moreover, the learned projection function from the hyperspectral data space to the RGB space can be directly applied to other hyperspectral images acquired by the same sensor to achieve a quick overview. Our method is also able to visualize user specified bands as natural color images, which is very helpful for users to scan bands of interest.**

***Index Terms*—Hyperspectral image, visualization, manifold alignment, image fusion**

I. Introduction

Hyperspectral imaging sensors can acquire images with tens or hundreds of light wavelength indexed bands. These images provide high spectral resolution information such that accurate target detection and classification can be achieved. Displaying a hyperspectral image (HSI) is a challenging task because it contains much more bands than the capability of a trichromatic display device. One common solution is considering HSI visualization as a special dimension reduction problem where the HSI is projected to the RGB color space to get a quick overview of a scene. Although the requirements of HSI visualization are task dependent, there are some common goals such as information preservation, consistent rendering, edge salience, and natural palette [1].

A simple way to generate an RGB image for HSI visualization is selecting three of the original bands and mapping them to the RGB space. Some softwares provide interactive tools for users to manually pick three bands [2], [3]. More sophisticated band selection methods, such as one-bit transform [4] and normalized information [5], aim to highlight expected features so that human perceptual channels are selected. In a more recent work, minimum estimated abundance covariance (MEAC) and linear prediction (LP) were used to select the most informative bands [6].

Some HSI visualization approaches condense the original spectral bands into three new bands by feature transformation. Several classic dimensionality reduction methods such as independent component analysis (ICA) [7] and principal component analysis (PCA) [8], [9], [10] have been applied to HSI visualization. However, these linear transformation methods are based on the global distribution of data, which ignore some intrinsic characteristics such as nonlinear and local structures of the HSI.

In recent years, manifold learning methods such as isometric feature mapping (ISOMAP) [11], [12], locality preserving projections (LPP) [13], and locally linear embedding (LLE) [14] have been applied to explore the manifold geometry in HSI. Manifold is a topological space that is locally Euclidean, i.e., it emphasizes the local neighborhood information. Similarly, some visualization methods aimed to preserve the pairwise distances between pixels in its visualized color image. This task is usually posed as a constrained optimization problem, but its heavy computational load is a critical challenge for real applications. Wilson et al. decreased the scale of the input data by selecting representative pixels and used numerical interpolation to generate the final optimization solution [15]. Mignotte used a non-stationary Markov random field (MRF) model to solve the optimization problem of preserving pairwise spectral distance [16], and later extended this approach to address the tradeoff between the preservation of spectral distances and the separability of features [17]. Edge information is also a significant local structure. Kotwal and Chaudhuria proposed to use nonlinear bilateral filtering with the edge preserving characteristic to calculate the band weights at each pixel for band image fusion [18]. These local structure based approaches demonstrate excellent performance in preserving the intrinsic information of HSI.

Most existing methods try to get the visualized image

D. Liao and Y. Qian are with the College of Computer Science, Zhejiang University, Hangzhou 310027, P.R. China. Corresponding author: Y. Qian (ytqian@zju.edu.cn)

J. Zhou is with the School of Information and Communication Technology, Griffith University, Nathan, Australia.

Y. Y. Tang is with the Faculty of Science and Technology, University of Macau, Macau 999078, China.

This work was supported by the National Basic Research Program of China 2012CB31640, the National Natural Science Foundation of China 61571393, 61273244, the Research Grants of University of Macau MYRG2015-00049-FST, MYRG2015-00050-FST, the Science and Technology Development Fund (FDCT) of Macau 100-2012-A3, 026-2013-A, the Australian Research Councils DECRA Projects funding scheme DE120102948.

convey as much information as possible from the original data. However, they do not enable easy image interpretation. The visualized RGB images of HSIs are falsely colored, which makes it difficult for human to link the color to the expected semantic meaning of land cover classes. For example, one may be confused when the grass is shown in red or the sea is shown in yellow. Moreover, the same objects/materials in different HSIs are often visualized in different colors, which also hinders the understanding of the image content. Therefore, "natural color" and "constant rendering" gradually become two important criteria for evaluating the quality of HSI visualization. "natural color" refers to the visible color that human visual system is able to perceive from a scene. When images are captured by imaging sensors with RGB channels, the formed colors are influenced by the sensor's sensitivity functions. In practice, visible imaging sensors only can capture approximate RGB images. The colors can be considered as natural so long as they are similar to human perception. In [1], [19], fixed linear spectral weighting envelope was introduced to generate a natural-looking image that rendered the same materials in different data sets with the same colors consistently. The spectral weighting envelope is a stretched version of the CIE 1964 tristimulus color matching functions in the visible range, which fits the cone responses of human visual system. However, the stretched color matching function (CMF) is too simple to represent the complex physical mechanism of spectral imaging, so that it is only applicable to some specific hyperspectral imaging sensors.

In most cases, both HSI and high resolution color image (HRCI) can be acquired on the same spot. These two types of images have strong complementary properties for information fusion. An HSI contains precise and detailed spectral information, but its spatial resolution is usually lower than the corresponding HRCI. On the other side, the appearance of an HRCI is consistent with the human visual perception, but an HSI is beyond our visual perception capability. It implies that the color information in an HRCI may be helpful in displaying the corresponding HSI with natural palette. This requires fusion of different presentations of the same object [20]. HSI and panchromatic image (PAN) fusion methods [21], [22] take advantage of the high spatial resolution of PAN in sharpening the HSI, which enhances the local spatial sharpness and contrast of the band images of the HSI. Pan-sharpening algorithms are also used in other applications such as object detection and classification [23], [24]. Recently, fusion of HSI and Light Detection And Ranging (LiDAR) images has also been studied [25], [26]. To the best of our knowledge, no research has been performed so far to visualize an HSI data by fusion it with an HRCI.

In this paper, we propose a novel HSI and HRCI fusion method based on manifold alignment to display the HSI with natural color. Manifold alignment is one of the important approaches for transfer learning [27], [28], which has been applied to multi-modal HSI processing and classification [29], [30], [31]. It builds connections between two or more disparate data sets by aligning their underlying manifolds and enables knowledge transfer across the data sets. We treat HSI and HRCI fusion based visualization as a transfer learning problem [32]. A shared space can be built to represent the manifolds of the HSI and the HRCI and their mutual relation. Via this shared space, the natural color distribution as well as the fine spatial information of the HRCI can be easily transferred to the HSI.

Generally there are two levels of manifold alignment: instance-level and feature-level [27]. Instance-level alignment builds connections between instances from different data sets, but the alignment result is limited only to known instances and is difficult to be generalized to new instances. Feature-level alignment transforms the features of different data sets to a common embedding space, which makes direct knowledge transfer possible. The alignment result provides direct connections between features in different spaces, so it is easily generalized to new instances. In this paper, the feature-level manifold alignment is used, where a direct mapping between the high dimensional spectral feature of the HSI and the RGB spectral feature of the HRCI is learned. The procedure of the proposed HSI visualization method has three main steps. Firstly, a few matching pixel pairs are detected between the HSI and the HRCI. Secondly, the manifolds of two images are aligned in a shared embedding space by forcing the matching pixels to be close to each other in the new space. Two projection functions are learned in this step to accomplish the space transformation task. One maps the HSI from the spectral space to the shared space, and the other maps the HRCI from the RGB space to the shared space. Finally, we inversely maps the manifold of the HSI in the shared space to the RGB space so that the HSI is displayed with natural color.

The main contributions and advantages of the proposed approach can be summarized as follows:

- Manifold alignment explores the manifolds of the HSI and the HRCI in a shared space simultaneously, so it not only preserves the local geometry of the HSI in the visualized image, but also renders the visualized image with natural color of the HRCI.
- The HSI is directly transformed to the RGB space, so that no additional color adjustment is required to fit the dynamic range of the trichromatic display and human visual expectation.
- The learned projection function from the spectral space to the RGB space can be reusable to visualize those HSIs that are acquired by the same hyperspectral imaging sensor.
- The proposed method can display any subset of bands selected by users with natural color, which is very important in interactive visualization.
- To align two manifolds, only a small number of matching pixel pairs between the HRCI and the HSI are needed rather than a precise registration between two images. Therefore, it is only required that the HSI and its corresponding HRCI have similar ground features, so they can be captured from different spots, which greatly decreases the cost of image acquisition and increases the usability of the approach.

The rest of the paper is organized as follows. Section II briefly introduces the manifold alignment technique. Sec-

tion III presents the manifold alignment based HSI visualization approach and the details of its implementation. Some application scenarios are also discussed in this section. The experimental results are described in Section IV. Finally, conclusions are drawn in Section V.

II. Background on Manifold alignment

It has been recognized that many high dimensional data lie on a low dimensional manifold embedded in the ambient space. Manifold learning is an effective dimension reduction method to extract nonlinear structures from high dimensional data. It maps a p-dimensional data set X to a q-dimensional data set Y, preserving the intrinsic geometry on the original manifold as much as possible. Manifold alignment considers the mutual relationships of several data sets at the same time. It generates a shared embedding space to represent the low-dimensional manifolds for all data sets simultaneously. In this section, manifold based dimension reduction is introduced, followed by the description of a manifold alignment algorithm.

A. Manifold based dimension reduction

Manifold based dimension reduction algorithms normally follow a similar procedure. The first step is building a sparse graph with k-nearest neighbors to represent the local geometry of a data set. This might include computing the shortest path between all points or figuring out how to linearly interpolate the point from its neighbors. Then a set of points in a low dimensional space are found, which preserve the properties of the original graph.

Here we briefly review the LPP algorithm [13], as the proposed manifold alignment algorithm for HSI visualization is extended from this model. LPP is a linear approximation of the nonlinear Laplacian Eigenmaps. Although LPP sacrifices the ability to represent arbitrarily warped manifolds, it is much faster than nonlinear manifold learning algorithms. This makes LPP based manifold alignment more suitable to process large amount of HSI data.

Given a data set represented by a matrix $\mathbf{X} \in R^{p\times n}$ where n is the number of samples, and p is the dimension of feature. Let $\mathbf{x}_i$ represent the ith sample in $\mathbf{X}$. LPP aims to find a linear transformation function $\mathbf{F} : R^p \rightarrow R^q$ to map each $\mathbf{x}_i$ from a p dimensional space to a q dimensional embedding space, where $q \ll p$.

Firstly, an adjacency graph G is constructed to represent the local geometry of $\mathbf{X}$. Each vertex in G represents a sample in the data set and each edge indicates the relationship between a pair of vertices. The relationship can be defined in terms of k-nearest neighbors, i.e., a pair of vertices i and j is connected by an edge if i is among the k nearest neighbors of j or j is among the k nearest neighbors of i. Let $\mathbf{W}$ with the size of $n \times n$ be the weighted adjacency matrix of G. The weight of an edge is calculated by heat kernel, a measurement widely used in graph construction to represent the geometric structure of data. The weight of an edge between the ith and the jth vertices is

$$\mathbf{W}(i,j) = \begin{cases} e^{\frac{-dist(\mathbf{x}_i,\mathbf{x}_j)}{\sigma^2}} & \text{if } \mathbf{x}_i \text{ and } \mathbf{x}_j \text{ are among the} \\ & \text{k-nearest neighbors of each other,} \\ 0 & \text{otherwise.} \end{cases} \tag{1}$$

where $dist(\mathbf{x}_i, \mathbf{x}_j)$ can be any application oriented distance metric between $\mathbf{x}_i$ and $\mathbf{x}_j$.

LPP aims at finding a linear projection matrix $\mathbf{F}$ with the size of $p \times q$ to map the data set from p-dimensional space to q-dimensional space. The objective function of LPP is formalized as:

$$E(\mathbf{F}) = \sum_{ij} \|\mathbf{F}^T\mathbf{x}_i - \mathbf{F}^T\mathbf{x}_j\|^2 \mathbf{W}(i,j) \tag{2}$$

where $\mathbf{F}^T\mathbf{x}_i$ are the coordinates of $\mathbf{x}_i$ in the low dimensional space. The sum is taken over all pairs of samples in the data set. Minimizing the objective function guarantees that the local geometry of the data set is preserved in the low dimensional space, i.e., two neighboring samples in the original space are still close to each other in the embedding space.

To find a solution to minimize Equation (2), the objective function can be reduced to

$$\begin{aligned} \frac{1}{2}E(\mathbf{F}) &= \frac{1}{2}\sum_{ij} \|\mathbf{F}^T\mathbf{x}_i - \mathbf{F}^T\mathbf{x}_j\|^2 \mathbf{W}(i,j) \\ &= \sum_i (\mathbf{x}_i^T\mathbf{F}\mathbf{D}_{ii}\mathbf{F}^T\mathbf{x}_i) - \sum_{ij}(\mathbf{x}_i^T\mathbf{F}\mathbf{W}_{ij}\mathbf{F}^T\mathbf{x}_j) \\ &= tr(\mathbf{F}^T\mathbf{X}(\mathbf{D}-\mathbf{W})\mathbf{X}^T\mathbf{F}) \\ &= tr(\mathbf{F}^T\mathbf{X}\mathbf{L}\mathbf{X}^T\mathbf{F}) \end{aligned} \tag{3}$$

$\mathbf{L} = \mathbf{D} - \mathbf{W}$ is the laplacian matrix of G where $\mathbf{D}$ is a diagonal matrix with $\mathbf{D}(i,i) = \sum_j \mathbf{W}(i,j)$. $tr()$ is the trace of a matrix. So the minimization problem can be rewritten as:

$$\arg\min_{\mathbf{F}} tr(\mathbf{F}^T\mathbf{X}\mathbf{L}\mathbf{X}^T\mathbf{F}) \tag{4}$$

which can be solved as the generalized eigenvalue problem

$$\mathbf{X}\mathbf{L}\mathbf{X}^T\mathbf{F} = \lambda\mathbf{X}\mathbf{D}\mathbf{X}^T\mathbf{F} \tag{5}$$

$\mathbf{F}$ is constructed by the q smallest eigenvectors because the matrices $\mathbf{X}\mathbf{L}\mathbf{X}^T$ and $\mathbf{X}\mathbf{D}\mathbf{X}^T$ are symmetric and positive semidefinite.

B. Feature-level manifold alignment

Manifold alignment is based on the assumption that seemingly disparate data sets produced by similar generating processes will share a similar underlying manifold structure. By projecting each data set from their original space to the shared manifold, connections can be built between disparate data sets by aligning their underlying manifolds [28]. The manifold alignment algorithm in this paper is based on LPP, which extends LPP from addressing single data set to several data sets. Here, we only introduce manifold alignment between two data sets. Generalizing the algorithm to more than two data sets is simple and straightforward.

Given two data sets represented by matrices $\mathbf{S} \in R^{p_s \times n_s}$ and $\mathbf{T} \in R^{p_t \times n_t}$ where n_s and n_t are the numbers of samples, and p_s and p_t are the dimensions of features. Let $\mathbf{x}_s^i$ represents the ith sample in $\mathbf{S}$, and $\mathbf{x}_t^j$ denotes the jth sample in $\mathbf{T}$. LPP based manifold alignment uses two linear projection functions $\mathbf{F}_s : R^{p_s} \to R^q$ and $\mathbf{F}_t : R^{p_t} \to R^q$ to transform two data sets from the original spaces to a shared embedding space R^q respectively. These two manifolds in the shared space are aligned by making the matching samples close to each other in this new space. The algorithm can be summarized as following steps:

1) Like the first step of LPP, construct two graphs G_s and G_t with the adjacency matrices $\mathbf{W}_s$ and $\mathbf{W}_t$ for two data sets respectively. $\mathbf{W}_s$ and $\mathbf{W}_t$ can be calculated by Equation (1).
2) Construct the correspondence matrix $\mathbf{W}_{st}$ by a set of matching pairs between two data sets to represent the corresponding relationship across two manifolds. The set of the matching pairs can be obtained by the prior or domain knowledge, or found by various matching algorithms [33], [34]. We will discuss the details of finding the matching pixels between the HSI and the HRCI in Section III-B. $\mathbf{W}_{st}$ is in the size of $n_s \times n_t$, the row of which indicates the indices of samples in $\mathbf{S}$, and the column indicates the indices of samples in $\mathbf{T}$. The entries of $\mathbf{W}_{st}$ can be defined as
$$\mathbf{W}_{st}(i,j) = \begin{cases} 1 & \text{if } \mathbf{x}_s^i \text{ and } \mathbf{x}_t^j \text{ form a matching pair} \\ 0 & \text{otherwise.} \end{cases} \tag{6}$$
3) Model manifold alignment problem by an objective function for computing the projection matrices $\mathbf{F}_s$ and $\mathbf{F}_t$. These two projection matrices transform two data sets from their original spaces to a shared embedding space. The objective function of manifold alignment can be designed as
$$\begin{aligned} E(\mathbf{F}_s, \mathbf{F}_t) = &\sum_{i,j} \|\mathbf{F}_s^T \mathbf{x}_s^i - \mathbf{F}_s^T \mathbf{x}_s^j\|^2 \times \alpha_1 \mathbf{W}_s(i,j) \\ &+ \sum_{m,n} \|\mathbf{F}_t^T \mathbf{x}_t^m - \mathbf{F}_t^T \mathbf{x}_t^n\|^2 \times \alpha_1 \mathbf{W}_t(m,n) \\ &+ \sum_{i,m} \|\mathbf{F}_s^T \mathbf{x}_s^i - \mathbf{F}_t^T \mathbf{x}_t^m\|^2 \times \alpha_2 \mathbf{W}_{st}(i,m) \end{aligned} \tag{7}$$
The first two terms on the right-hand side guarantee that the local geometry of each given data set is preserved, i.e., similar samples from the same data set are still close to each other in the shared space. The last term ensures that the matching samples from different data sets are close to each other in the shared space. Parameters α_1 and α_2 control the balance between local geometry preserving and manifold alignment.
4) Solve the problem of minimizing $E(\mathbf{F}_s, \mathbf{F}_t)$. We generate a joint graph G with G_s and G_t. Its vertices represent the union of $\mathbf{S}$ and $\mathbf{T}$. Its weighted adjacency matrix $\mathbf{W}$ is defined as
$$\mathbf{W} = \begin{bmatrix} \alpha_1 \mathbf{W}_s & \alpha_2 \mathbf{W}_{st} \\ \alpha_2 \mathbf{W}_{st}^T & \alpha_1 \mathbf{W}_t \end{bmatrix} \tag{8}$$
where $\mathbf{W}_{st}^T$ is the transpose of $\mathbf{W}_{st}$. It can be seen that $\mathbf{W}$ is an $(n_s+n_t)\times(n_s+n_t)$ symmetric matrix. Specifically, the entries of $\mathbf{W}$ are defined as
$$\mathbf{W}(i,j) = \begin{cases} \alpha_1 \mathbf{W}_s(i,j) \text{ or } \alpha_1 \mathbf{W}_t(i,j) & \text{if } \mathbf{x}_i \text{ and } \mathbf{x}_j \text{ are neighbors from the same data set,} \\ \alpha_2 \mathbf{W}_{st}(i,j) & \text{if } \mathbf{x}_i \text{ and } \mathbf{x}_j \text{ are the matching pixels from two data sets,} \\ 0 & \text{otherwise.} \end{cases} \tag{9}$$
Now Equation (7) can be rewritten as
$$E(\mathbf{F}) = \sum_{ij} \|\mathbf{F}^T \mathbf{x}_i - \mathbf{F}^T \mathbf{x}_j\|^2 \mathbf{W}(i,j) \tag{10}$$
where $\mathbf{F} = [\mathbf{F}_s; \mathbf{F}_t]$ contains $\mathbf{F}_s$ and $\mathbf{F}_t$ in row blocks, and the summation is taken over all pairs of samples from the united data set $\mathbf{X} = \mathbf{S} \cup \mathbf{T}$. Obviously Equation (10) is very similar to Equation (2), so the $\mathbf{F}$ that minimizes the objective function is given by the eigenvectors corresponding to the q smallest nonzero eigenvalues of the generalized eigenvalue decomposition:
$$\mathbf{X}\mathbf{L}\mathbf{X}^T\mathbf{F} = \lambda \mathbf{X}\mathbf{D}\mathbf{X}^T\mathbf{F} \tag{11}$$
where $\mathbf{L}$ is the Laplacian form of $\mathbf{W}$.
5) Derive two aligned manifolds in a shared space by $\mathbf{F}^T\mathbf{S}_s$ and $\mathbf{F}^T\mathbf{T}_t$ respectively. As the estimated $\mathbf{F}$ has the size of $(p_s + p_t) \times q$, $\mathbf{F}_s$ is constructed by the first p_s rows of $\mathbf{F}$ and $\mathbf{F}_t$ is constructed by the last p_t rows of $\mathbf{F}$.

By manifold alignment, the data sets are represented in a shared feature space, so that the processing of several disparate but related data sets becomes easy for various applications. This is because they can be directly and consistently addressed in the shared space, i.e., they can be treated as a single data set.

III. Manifold alignment based HSI visualization

This section covers the details of manifold alignment based HSI visualization method. Firstly, the basic methodology is introduced. Then the key implementation issue of how to obtain the matching pairs is studied when both the HSI and the HRCI are captured from the same site, Finally, other visualization scenarios are discussed.

A. Methodology

Given an HSI and an HRCI, Fig. 1 summarizes the workflow of the manifold alignment based visualization approach. Firstly, a set of matching pixel pairs are found between the HSI and the HRCI to build the relation between two images. Secondly, LPP based manifold alignment is used to derive the manifolds of two images in a shared space. Two linear transformations denoted as the projection matrices $\mathbf{F}_s$ and $\mathbf{F}_t$ are estimated to

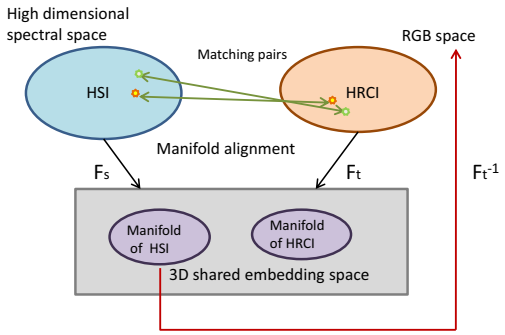

Fig. 1. The workflow of the proposed visualization method.

map the HSI and the HRCI from their original spaces to the shared embedding space respectively. Finally, the manifold of the HSI in the shared space is mapped to the RGB space by the inverse transformation of $\mathbf{F}_t$.

Assume an HSI has n_s pixels and p_s spectral bands, and the corresponding HRCI has n_t pixels and $p_t = 3$ RGB bands, so the HSI data set and the HRCI data set can be denoted by the matrices $\mathbf{S} \in R^{n_s \times p_s}$ and $\mathbf{T} \in R^{n_t \times P_t}$ respectively. We use $\mathbf{s}_i$ to denote the ith pixel in the HSI and $\mathbf{t}_j$ to denote the jth pixel in the HRCI. The proposed visualization algorithm consists of the following steps.

Step 1: Construct graphs G_s and G_t.

The vertex sets of G_s and G_t are the pixels of the HSI and the HRCI respectively, and their weighted adjacency matrices $\mathbf{W}_s$ and $\mathbf{W}_t$ are defined by the k-nearest neighbor and the heat kernel. Since the HSI and the HRCI have distinct imaging mechanism, we use different distance measures in the heat kernel. As the spectral angle distance (SAD) is commonly used to measure the distance of a pair of pixels in HSI, the entries of the weighted adjacency matrix of the HSI are defined as

$$\mathbf{W}_s(i,j) = e^{\frac{-SAD(\mathbf{s}_i,\mathbf{s}_j)}{\sigma}} \tag{12}$$

where

$$SAD(\mathbf{s}_i,\mathbf{s}_j) = \arccos\left(\frac{\mathbf{s}_i \cdot \mathbf{s}_j}{\|\mathbf{s}_i\|\|\mathbf{s}_j\|}\right) \tag{13}$$

On the other hand, Euclidean distance is used for the HRCI, so its weights are defined as

$$\mathbf{W}_t(i,j) = e^{\frac{-\|\mathbf{t}_i-\mathbf{t}_j\|^2}{\sigma}} \tag{14}$$

Step 2: Calculate the correspondence matrix $\mathbf{W}_{st}$.

The matching pairs play a crucial role in aligning the manifolds of the HSI and the HRCI in a shared embedding space. If the HSI and its corresponding HRCI are acquired on the same site, we can search their matching relation by the image registration methods, which will be discussed in Section III-B. If the HSI and its corresponding HRCI are captured from the different sites but have the similar contents, interactive tool can be used to find the matching pairs, which will be discussed in Section III-C.

After a set of matching pairs is determined, the correspondence matrix $\mathbf{W}_{st}$ with the size of $n_s \times n_t$ is defined as

$$\mathbf{W}_{st}(i,j) = \begin{cases} 1 & \text{if } \mathbf{s}_i \text{ and } \mathbf{t}_j \text{ form a matching pair.} \\ 0 & \text{otherwise.} \end{cases} \tag{15}$$

Step 3: Solve LPP based manifold alignment problem.

G_s of the HSI and G_t of the HRCI are joined to generate a new graph G. Its weighted adjacency matrix $\mathbf{W}$ is the combination of $\mathbf{W}_s$, $\mathbf{W}_t$, and $\mathbf{W}_{st}$ according to Equation (8). Deriving two aligned manifolds of the HSI and the HRCI simultaneously in a shared embedding space is an optimization problem with the objective function defined in Equation (10). Likewise, the generalized eigenvalue decomposition is used to solve this optimization problem. Two linear transformation matrices $\mathbf{F}_s$ and $\mathbf{F}_t$ are computed, and by which the manifolds of the HSI and the HRCI in the shared space can be obtained as $\mathbf{S}_c = \mathbf{F}_s^T\mathbf{S}$ and $\mathbf{T}_c = \mathbf{F}_t^T\mathbf{T}$ respectively.

As the feature dimension of the HRCI is 3, the dimension of the shared space can be 1, 2 or 3 theoretically. Here the dimension of the shared space is set to 3 in order to guarantee that an inverse projection of $\mathbf{F}_t$ can be directly computed because $\mathbf{F}_t$ is a square matrix with the size of 3×3.

Step 4: Transform the HSI to the RGB space.

After manifold alignment, the manifolds of the HSI and the HRCI are represented in the same space. The pixels of the HRCI in the shared space can be seen as anchor points. If a pixel of the HSI is close to a pixel of the HRCI in the shared space, obviously this HSI pixel should be rendered with the similar color of the corresponding HRCI pixel. In other words, a pixel in the HSI can find its corresponding RGB color in the shared space. Since $\mathbf{F}_s$ and $\mathbf{F}_t$ have been obtained to transform the high dimensional spectral space and the RGB space respectively to the shared space, we can inversely transform a pixel of HSI from the shared space to the RGB space by $\mathbf{F}_t^{-1}$. Therefore, the visualized HSI denoted as $\mathbf{S}_{rgb}$ can be obtained by

$$\mathbf{S}_{rgb} = (\mathbf{F}_t^{-1})^T\mathbf{S}_c = (\mathbf{F}_t^{-1})^T\mathbf{F}_s^T\mathbf{S} \tag{16}$$

B. Finding the matching pairs between HSI and HRCI

In many instances, an HSI and its corresponding HRCI have to be matched by image registration. In general, an image registration method firstly finds a few corresponding pixel pairs, and then uses them to estimate a geometric transformation model so that two images are matched in the same coordinate system. Scale-invariant feature transform (SIFT) is widely used to detect the corresponding pixels between images due to its robustness to changes in scale, orientation and illumination [35]. We extract the SIFT key-points from each band image of the HSI and the HRCI. Assume that a set SP contains the key-points from all the bands of the HSI, and another set TP has all the key-points from the HRCI. Let SP_i denotes the ith key-point in SP, and TP_j denotes the jth key-point in TP. The corresponding pairs are those most similar key-point pairs between SP and TP, which shall satisfy the following criterion.

$$\frac{dis(SP_i,TP_k)}{dis(SP_i,TP_j)} > r \quad \text{for all } k \neq j \tag{17}$$

where $dis(SP_i,TP_j)$ is the Euclidean distance between the SIFT features of SP_i and TP_j. r is a matching threshold value, which is set to be larger than 1. This criterion can rule out ambiguous matches because SP_i and TP_j are matched

only when their SIFT distance is significantly smaller than the distance between SP_i and all other key-points in TP.

We used projective transformation to estimate the geometric transformation models.

$$(x', y', 1)^{\mathrm{T}} = \mathbf{H}(x, y, 1)^{\mathrm{T}} \tag{18}$$

where $\{(x, y), (x', y')\}$ stands for the coordinates of a matching pair between the HSI and the HRCI, and

$$\mathbf{H} = \begin{pmatrix} h_1 & h_2 & h_3 \\ h_4 & h_5 & h_6 \\ h_7 & h_8 & 1 \end{pmatrix} \tag{19}$$

is the transformation matrix, or called homography matrix. If we find n matching pairs $\{(x_i, y_i), (x'_i, y'_i)\}, i = 1, \ldots, n$ by SIFT matching, $\mathbf{H}$ can be estimated by

$$\min_{\mathbf{H}} \sum_{i=1}^{n} \|(x'_i, y'_i, 1)^{\mathrm{T}} - \mathbf{H}(x_i, y_i, 1)^{\mathrm{T}}\|^2. \tag{20}$$

Since there are eight parameters in $\mathbf{H}$, at least four non-colinear matching pairs are required to solve Equation (20). Least squares technique is used to estimate these model parameters. To cope with mismatched pairs, we used RANdom SAmple Consensus (RANSAC) technique [36], [37] to give a more robust model estimation.

After image registration, each pixel in the HSI can find its matching in the HRCI. We can randomly select a number of pixels in the HSI, and find their matching pixels in the HRCI to construct a set of matching pixel pairs. However, precise image registration between the HSI and the HRCI is very difficult to obtain. Here neighborhood searching is used to improve the matching accuracy. Given a pixel $\mathbf{s}_i$ in the HSI, a pixel in the neighborhood window in the HRCI with the minimal SIFT distance to $\mathbf{s}_i$ is selected as the matching pixel. In our experiments, the size of window was set to 9×9. It is an distinct advantage that an exact registration between the HSI and the HRCI is not necessary, which is very helpful in real applications.

C. Other visualization scenarios

Besides displaying an HSI aided by a corresponding HRCI acquired on the same site, the proposed HSI visualization algorithm can be easily extended to other scenarios.

Generalizing projection functions to visualize other similar HSIs: Feature-level manifold alignment builds the relations between features from different spaces so that it can be easily generalized to new instances and provides a "dictionary" representing direct mapping functions between features [27]. For HSI visualization task, the projection function from high dimensional spectral space to the RGB space is defined as $\mathbf{F} = \mathbf{F}_s \mathbf{F}_t^{-1}$, where $\mathbf{F}_s$ and $\mathbf{F}_t$ are acquired by the manifold alignment discussed in section III-A. This projection function can be directly applied to visualize other similar HSIs captured by the same hyperspectral imaging sensor, which is based on the fact that the same types of objects shall have similar spectral responses with the same sensor. This scenario is very helpful when users require a quick overview of a batch of HSIs generated by the same imaging sensor, because the projection function learning only need to be undertaken for once.

Manifold alignment between an HSI and an HRCI from different sites: In the absence of a corresponding HRCI captured from the same site as an HSI to aid visualization, other HRCIs containing similar image content can be used instead for manifold alignment. Under such scenario, matching pair search method based on image registration as described in Section III-B is not applicable. However, manifold alignment based visualization only requires that a matching pair represents the same or similar class of objects/materials rather than from the same geo-spatial location. This is different from the traditional matching pair searching in image fusion. Therefore, interactive tools can be developed for users to manually select the matching pixels.

Displaying user specified bands: Interactive visualization allows users to display selected bands of interests, which is an important function in most HSI visualization tools. The proposed algorithm is able to present user specified bands as a natural-looking image. This is achieved by manifold alignment between the selected bands and the corresponding HRCI. In this case, the choice of bands is flexible so long as their total number is larger than or equal to 3. As most existing visualization options that have been integrated into commercial softwares only allow selection of three bands for visualization, some range of spectrum will be missed when an HSI covers a wide range of spectrum. On the contrary, our method offers the capability of getting a wide range of spectrum covered when more than 3 bands are selected.

IV. Experiments and discussions

We evaluate the performance of the proposed visualization method on HSIs captured by remote sensing and ground-based hyperspectral sensing, and compare it against several recently proposed visualization approaches. These include band selection using linear prediction (LP) [6], stretched CMF [1], bilateral filtering [18], bicriteria optimization [17] and LPP [13]. The impact of parameters on the performance, e.g. the number of corresponding pairs and the weight of the alignment between the matching pixels, is discussed. We also give the experimental results on various application scenarios.

A. Hyperspectral imaging data

Four HSI data sets were used to evaluate the performance of different visualization methods. Their corresponding HRCIs were captured from the same sites. One remote sensing HSI data set was taken over Washington D.C. mall by the Hyperspectral Digital Imagery Collection Experiment (HYDICE) sensor. The data consists of 191 bands after noisy bands removed, in which the size of each band image is 1208×307. Fig. 2(a) shows its 50th band image. The corresponding HRCI of Washington D.C. mall was obtained from Google Earth and is shown in Fig. 2(b). The size of the image is 5160×1640. Another remote sensing HSI data set was captured by the Airborne Visible/Infrared Imaging Spectrometer (AVIRIS) over Moffett Field, California at the southern end of San Francisco Bay. The data consists of 224 bands, and each band is in the

size of 501×651. Its 50th band image is shown in Fig. 3(a). The corresponding HRCI shown in Fig. 3(b) was also obtained from Google Earth. The size of the image is 1560×1830.

Other two HSI data sets are named as "G03" and "D04", which were acquired by a ground-based OKSI hyperspectral imaging system mounted with a tunable LCTF filter. Each data set has 18 bands ranging from $460nm$ to $630nm$ at $10nm$ interval. The size of each band is 960×1280. Their corresponding HRCIs were acquired by a Nikon D60 SLR digital camera, and are in the size of 2592×3872. Fig. 4 shows the first band images of these two ground-based HSIs and their corresponding HRCIs.

B. Visual comparison of visualization methods

To evaluate the visualization results, both subjective visual judgment and objective metrics are used. In this subsection, we show the visual effect of the HSI visualization results. Fig. 5 shows the visual comparison of different visualization approaches on the Washington D.C. mall data. The visualized image generated by manifold alignment is presented in Fig. 5(f). It was achieved by selecting 20 matching pairs and setting the parameters α_1 and α_2 to be 1 and 500 respectively. It can be seen that the result of manifold alignment not only has a very natural tone but also preserves fine details.

The comparative results on Moffett field, G03 and D04 data sets are provided in Figs. 6, 7 and 8 respectively. Likewise, in these experiments our approach not only shows great performance on displaying these images with natural color but also preserves finer details with accuracy.

C. Quantitative comparison of visualization methods

Quantitative assessment of HSI visualization does not have a universally accepted standard. In this paper, we adopt four quantitative metrics: entropy [18], average gradient [18], separability of features [38], and root mean square error (RMSE) between the resultant image and the true color image [7].

- Entropy

Entropy is a statistical measure of randomness that can be used to characterize the texture of an image. An image with higher entropy contains richer information than ones with low entropy. The entropy of a single channel image is given by:

$$h = -\sum_x p(x) \ln p(x) \tag{21}$$

where $p(x)$ is the probability density of the intensity level x in the image. For an RGB image, its entropy is the average entropy of R, G and B channels.

Table I shows the comparative results in terms of entropy. It can be found that in most cases the manifold alignment method has larger entropy than other approaches, which suggests that the proposed method can preserve more information of HSI in its RGB form.

- Average gradient

Average gradient is the measure of image sharpness in terms of gradient values [38]. For a single channel image with N pixels, let I_x denote the difference in the x-axis direction and I_y denote the difference in the y-axis direction, the average gradient of image is given by

$$\overline{g} = \frac{1}{N} \sum_x \sum_y (\sqrt{I_x^2 + I_y^2}) \tag{22}$$

TABLE I
PERFORMANCE COMPARISON BASED ON ENTROPY.

Visualization methods	Washington	Moffett	G03	D04
LP Band Selection	6.59	6.36	4.73	5.58
LPP	6.53	5.99	5.11	6.15
Stretched CMF	3.89	5.28	6.31	7.13
Bilateral Filtering	3.31	5.87	6.05	**7.27**
Bicriteria Optimization	5.75	6.00	5.73	6.06
Manifold Alignment	**7.40**	**6.89**	**6.64**	7.02

Table II gives the comparative results in terms of the average gradients on R, G and B channels. It is found that in two data sets the proposed approach yields the higher average gradient than other methods.

- Separability of features

When many pixels in an image fall within a small range of the color space, the image will be too dark or too bright. Separability of features measures how well distinct pixels are mapped to distinguishable colors. The basic idea is that the average distance between two pixels in the color space should be as large as possible [38]. Separability of features is defined as:

$$\delta = \frac{1}{(N-1)^2} \sum_{x \neq y} d(x, y) \tag{23}$$

where $d(x, y)$ is the Euclidean distance between the pair of pixels x and y in the RGB space, N is the number of pixels. δ denotes the average pairwise Euclidean distance in terms of all pixel pairs. The larger δ, the better separability of features.

Table III shows the comparative results in terms of feature separability. The good performance of manifold alignment is achieved by the high dynamic color range of the corresponding HRCI.

- RMSE

RMSE between the true color image and the visualized image is a straightforward way to evaluate the visualization performance [7]. We approximated a true color image by resizing the HRCI to the same size/resolution of the HSI after image registration. Let $s(x)$ denote the RGB vector of pixel x in the visualized image, and let $s'(x)$ represent the vector of the corresponding pixel in the true color image. The RMSE between s and s' over the whole image is defined by:

$$r = \sqrt{\frac{1}{N} \sum_x (s(x) - s'(x))^2} \tag{24}$$

The comparative results of RMSE are given in Table IV. The proposed method is significantly better than the other ones on all four data sets, which shows clearly that manifold alignment is an excellent approach for visualizing the HSI with natural color.

TABLE II
PERFORMANCE COMPARISON BASED ON AVERAGE GRADIENT.

Visualization methods	Washington	Moffett	G03	D04
LP Band Selection	0.0470	0.0109	0.0137	0.0151
LPP	0.0527	0.0078	0.0176	0.0125
Stretched CMF	0.0192	0.0049	0.0116	0.0106
Bilateral Filtering	0.0448	0.0088	0.0203	0.0210
Bicriteria Optimization	0.0387	**0.0122**	0.0217	**0.0283**
Manifold Alignment	**0.0889**	0.0103	**0.0270**	0.0219

TABLE III
PERFORMANCE COMPARISON BASED ON SEPARABILITY OF FEATURES.

Visualization methods	Washington	Moffett	G03	D04
LP Band Selection	55.68	51.33	63.25	135.37
LPP	78.99	42.12	39.82	50.87
Stretched CMF	30.08	30.44	106.14	73.30
Bilateral Filtering	47.54	51.80	82.16	143.19
Bicriteria Optimization	52.43	62.51	122.78	**168.65**
Manifold Alignment	**107.11**	**65.23**	**139.58**	107.81

TABLE IV
PERFORMANCE COMPARISON BASED ON RMSE

Visualization methods	Washington	Moffett	G03	D04
LP Band Selection	68.35	49.93	95.19	83.35
LPP	90.96	63.97	108.44	108.02
Stretched CMF	92.46	58.50	44.09	28.70
Bilateral Filtering	102.43	56.70	78.54	61.14
Bicriteria Optimization	98.47	57.94	69.60	75.70
Manifold Alignment	**58.41**	**27.30**	**32.88**	**23.08**

TABLE V
QUANTITATIVE COMPARISON OF VISUALIZATION RESULTS OF D04.

Visualization methods	Entropy	Gradient	Separability	RMSE
LP Band Selection	5.59	0.0151	135.37	83.35
LPP	6.15	0.0125	50.87	108.02
Stretched CMF	7.13	0.0106	73.30	**28.70**
Bilateral Filtering	7.26	0.0210	143.19	61.14
Bicriteria Optimization	6.06	0.0283	**168.65**	75.70
Manifold Alignment	**7.50**	**0.0350**	147.54	58.47

D. Parameter setting

Now we turn to discuss how the parameters affect the performance of manifold alignment and how to set suitable parameters to achieve a reasonable visualization result. In the proposed algorithm, if we fix $\alpha_1 = 1$, there are two free parameters. One is the number of matching pairs denoted as N_{cp}, and the other is the weight factor α_2 which controls how much two data sets would be aligned. To analyze the impact of α_2, we did experiments on the Washington D.C. mall HSI with different α_2 while fixing $\alpha_1 = 1$ and $N_{cp} = 20$. Fig. 9 displays the visualized results with $\alpha_2 = 100, 500$ respectively. We observed that as α_2 becomes larger, the color distribution of the visualized image is more similar to that of the HRCI. It should be noted that when α_2 is set to a very large value, the accuracy of matching pairs becomes very critical, because even a small number of mismatching pairs will lead to an undesirable result. Based on the experiments, reasonable results can be achieved in most cases by setting α_2 to be $200 - 500$.

Next we analyze the impact of the number of matching pairs. In this experiment, we fix $\alpha_1 = 1$ and $\alpha_2 = 500$. Fig. 10(a) is the visualization result by randomly selecting 5 matching pixel pairs. It can be observed that only using 5 matching pairs is still able to make the visualized image appear very natural. When the number of matching pairs is set to 30, the image not only has more natural colors but also has more detailed spatial information as shown in Fig. 10(b). This experiment supports the fact that only a few matching pairs between the HSI and the HRCI are sufficient for manifold alignment.

In addition, two parameters discussed above have some relations. It has been found that when the number of matching pairs becomes larger, α_2 should be tuned down to achieve a reasonable visualization result. This is because of the tradeoff between preserving each manifold structure and aligning two manifolds, which is controlled by α_2 and N_{cp} when estimating the manifolds in the shared space.

(a) The 50th band of the HSI

(b) The corresponding HRCI

Fig. 2. An HSI and its corresponding HRCI on Washington D.C. mall

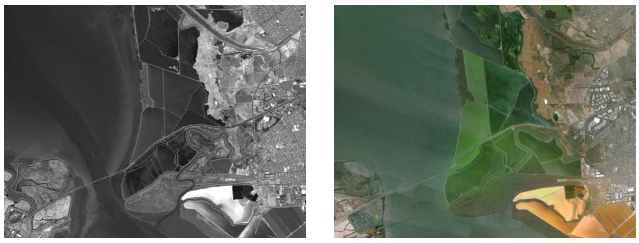

(a) The 50th band of the HSI (b) The corresponding HRCI

Fig. 3. An HSI and its corresponding HRCI on Moffett Field

E. Generalizing projection function to other HSIs

Once we have obtained a projection function by manifold alignment based on an HSI and its corresponding HRCI captured from the same site, this projection function can be directly used to visualize HSIs captured by the same hyperspectral imaging sensor when their corresponding HRCIs are not available. In this experiment, the projection function derived from G03 data set and its corresponding HRCI, was applied to other HSI data sets F02, G04 and G02 captured by the same HSI camera. Fig. 11 shows the visualized images of these four HSI data sets, which were generated by directly multiplying the data matrix with the projection matrix $\mathbf{F} = \mathbf{F}_s\mathbf{F}_t^{-1}$. It can be seen that these images are rendered with natural color.

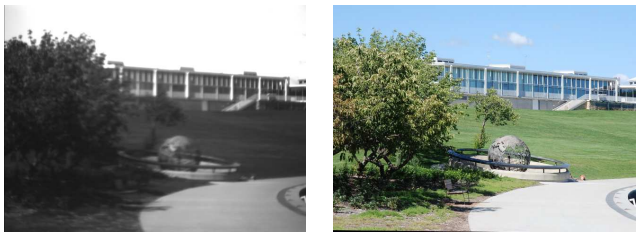

(a) The first band of D04 (b) The HRCI of D04

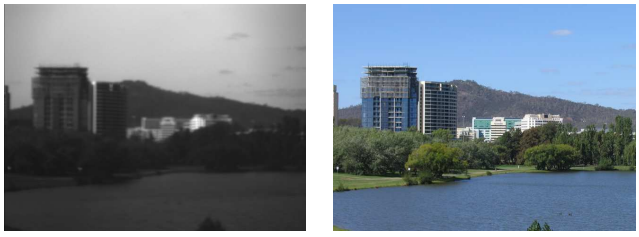

(c) The first band of G03 (d) The HRCI of G03

Fig. 4. Two ground-based HSIs and their corresponding HRCIs

F. Manifold alignment between the HSI and the HRCI captured from different sites

We used the D04 HSI data set (Fig. 12(a)) and the HRCI of G03 (Fig. 4(d)) for manifold alignment. These images were captured from the different sites. Fourteen matching pixel pairs between two images were manually selected. Fig. 12(b) shows the visualized image of D04. Although the details in this image are not as fine as the result of manifold alignment with the HRCI from the same site (Fig. 8(f)), the image is also mostly rendered with natural color. We can easily recognize the objects in it such as the sky, trees and grass. Table V gives the quantitative comparison of visualization results of HSI D04 generated by different methods. We can see that the proposed method has the highest entropy and average gradient, and ranks second in terms of separability of features and RMSE.

G. Displaying user specified channels by manifold alignment

Fig. 13(a) shows a false color image of band 58, 80 and 120 of the Washington D.C. mall data set by simply integrating them to RGB channels. The colors of the visualized image cannot reflect the natural tones of the objects, which affects object recognition and interpretation. For example, the roads in the image are difficult to recognize because their colors are similar to the surrounding areas. Fig. 13(b) shows the visualized image generated by manifold alignment between a new HSI constructed by the selected bands and the corresponding HRCI. It can be found that the visualized image is rendered with natural color. In particular, the roads are more distinguishable from the neighborhood, which also demonstrates that our approach can make use of a wider range of color space in the HRCI to produce higher color separability.

V. Conclusions

We have presented a new approach to visualize HSIs with natural color. Based on manifold alignment between an HSI and an HRCI, the proposed algorithm is able to find a projection function that maps the HSI directly from high-dimensional spectral space to the RGB space. The matching pixel pairs between the HSI and the HRCI act as a bond to transfer the color information as well as local geometric information from the HRCI to the HSI. The main advantage of the proposed algorithm is that only a few matching pairs are required to achieve a satisfactory result. This suggests that exact image registration is not a necessary condition to extract the matching pairs. Therefore, even in the case that the HSI and the HRCI are not captured over the same site, our method still works well. Furthermore, by projecting the HSI directly to the RGB space, our algorithm avoids spectral distances distortion that other methods have suffered from while adjusting data to the dynamic range of RGB. The projection function learned from the HSI and its corresponding HRCI can be directly applied to visualization of other HSIs captured by the same imaging sensor. In addition to these advantages, manifold

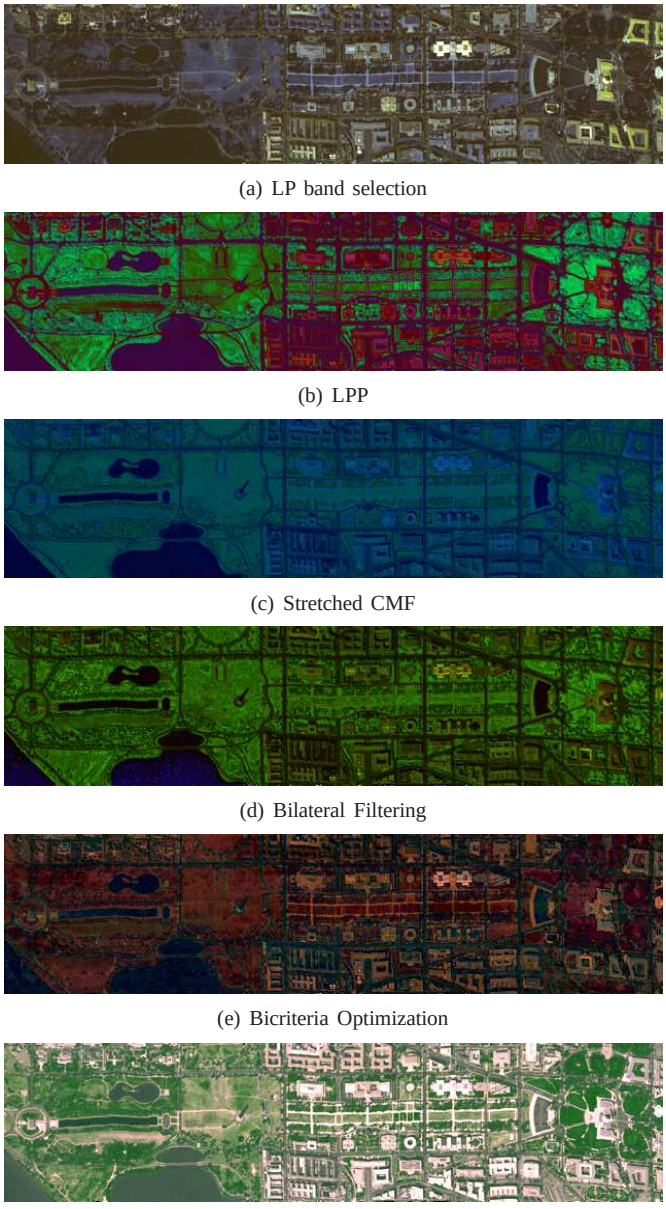

(a) LP band selection

(b) LPP

(c) Stretched CMF

(d) Bilateral Filtering

(e) Bicriteria Optimization

(f) Manifold Alignment

Fig. 5. Visual comparison of various visualization approaches on Washington D.C. mall data set.

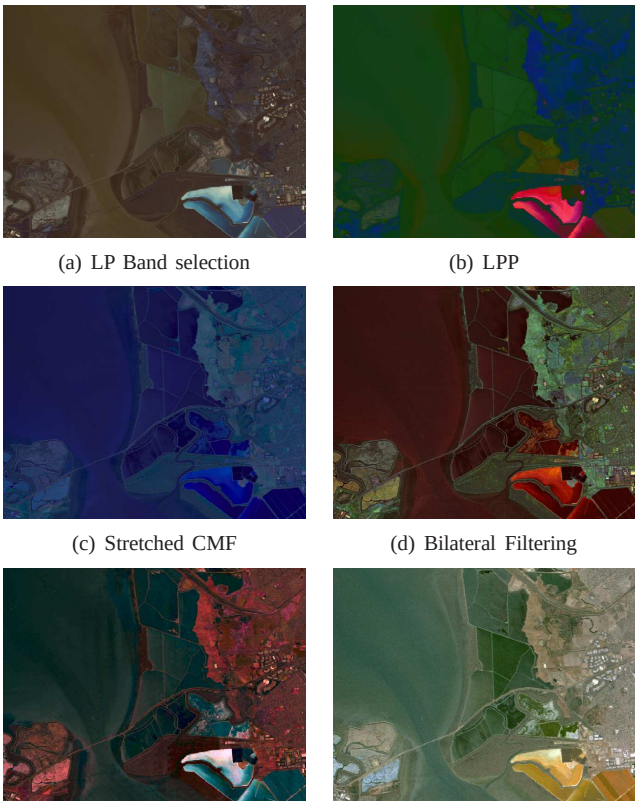

(a) LP Band selection (b) LPP

(c) Stretched CMF (d) Bilateral Filtering

(e) Bicriteria Optimization (f) Manifold Alignment.

Fig. 6. Visual comparison of various visualization approaches on Moffett field data set.

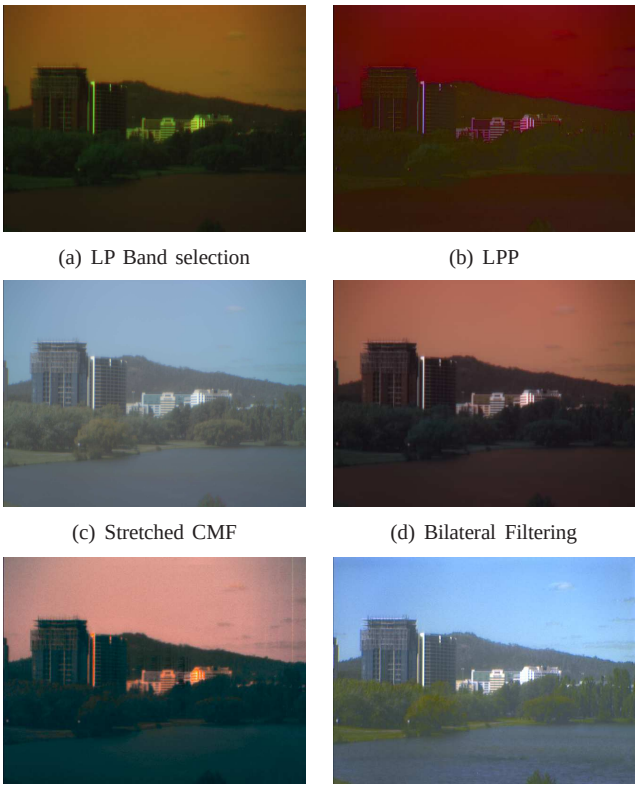

(a) LP Band selection (b) LPP

(c) Stretched CMF (d) Bilateral Filtering

(e) Bicriteria Optimization (f) Manifold Alignment

Fig. 7. Visual comparison of various visualization approaches on G03 data set.

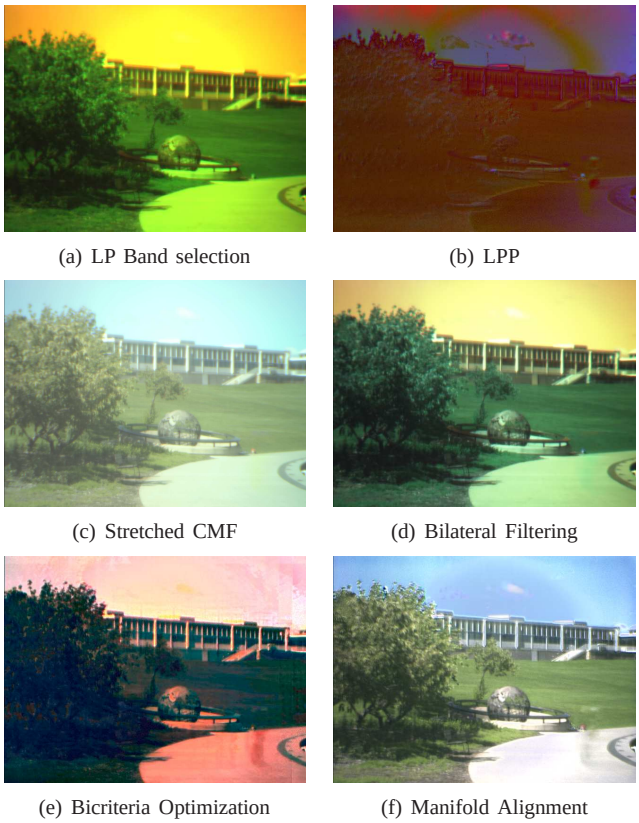

(a) LP Band selection (b) LPP

(c) Stretched CMF (d) Bilateral Filtering

(e) Bicriteria Optimization (f) Manifold Alignment

Fig. 8. Visual comparison of various visualization approaches on D04 data set.

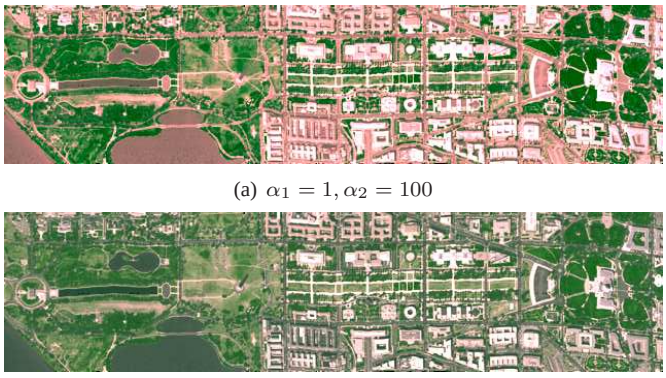

(a) $\alpha_1 = 1, \alpha_2 = 100$

(b) $\alpha_1 = 1, \alpha_2 = 500$

Fig. 9. The visualization results with different values of α_2 in manifold alignment.

alignment can be used to display user specified bands, which is very important to develop an interactive visualization tool. In the future, constrained manifold alignment algorithms will be studied to visualize HSIs by adding more transformation constraints such as pairwise distance preservation and joint spectral-spatial structure.

REFERENCES

[1] N. P. Jacobson and M. R. Gupta, "Design goals and solutions for display of hyperspectral images," *IEEE Trans. Geosci. Remote Sens.*, vol. 43, no. 11, pp. 2684–2692, 2005.

[2] MultiSpec. [Online], Available:http://cobweb.ecn.purdue.edu/biehl/multispec/description.htm.

[3] ENVI. [Online], Available:http://www.ittvis.com/envi/.

(a) Number of matching pairs = 5

(b) Number of matching pairs = 30

Fig. 10. The visualization results with different numbers of matching pairs.

(a) The first band of F02

(b) Visualized image of F02

(c) The first band of G04

(d) Visualized image of G04

(e) The first band of G02

(f) Visualized image of G02

Fig. 11. Generalizing projection function to other HSI data sets.

(a) The first band of D04

(b) Visualized image of D04

Fig. 12. Visualized image of D04 generated by aligning with the HRCI captured from a different site.

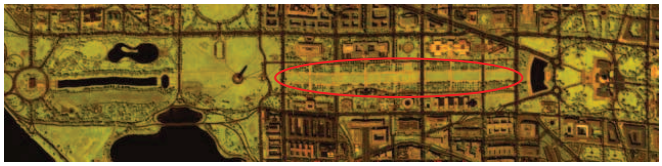

(a) False color image of bands 58, 80, 120.

(b) Visualized image of bands 58, 80, 120 by manifold alignment.

Fig. 13. Displaying specified bands of Washington D.C. mall HSI data set.

[4] B. Demir, A. Celebi, and S. Erturk, "A low-complexity approach for the color display of hyperspectral remote-sensing images using one-bit-transform-based band selection," *IEEE Trans. Geosci. Remote Sens.*, vol. 47, no. 1, pp. 97–105, 2009.

[5] S. Le Moan, A. Mansouri, Y. Voisin, and J. Y. Hardeberg, "A constrained band selection method based on information measures for spectral image color visualization," *IEEE Trans. Geosci. Remote Sens.*, vol. 49, no. 12, pp. 5104–5115, 2011.

[6] H. Su, Q. Du, and P. Du, "Hyperspectral image visualization using band selection," *IEEE J. Select. Topics Appl. Earth Observ. Remote Sens.*, vol. 7, no. 6, pp. 2647–2658, 2014.

[7] Y. Zhu, P. K. Varshney, and H. Chen, "Evaluation of ica based fusion of hyperspectral images for color display," in *Proc. Int. Conf. Inf.Fusion*, 2007, pp. 1–7.

[8] J. S. Tyo, A. Konsolakis, D. I. Diersen, and R. C. Olsen, "Principal-components-based display strategy for spectral imagery," *IEEE Trans. Geosci. Remote Sens.*, vol. 41, no. 3, pp. 708–718, 2003.

[9] C.-I. Chang and Q. Du, "Interference and noise-adjusted principal components analysis," *IEEE Trans. Geosci. Remote Sens.*, vol. 37, no. 5, pp. 2387–2396, 1999.

[10] Q. Du, N. Raksuntorn, S. Cai, and R. J. Moorhead, "Color display for hyperspectral imagery," *IEEE Trans. Geosci. Remote Sens.*, vol. 46, no. 6, pp. 1858–1866, 2008.

[11] C. M. Bachmann, T. L. Ainsworth, and R. A. Fusina, "Exploiting manifold geometry in hyperspectral imagery," *IEEE Trans. Geosci. Remote Sens.*, vol. 43, no. 3, pp. 441–454, 2005.

[12] S. A. Najim, I. S. Lim, P. Wittek, and M. W. Jones, "Fspe: Visualization of hyperspectral imagery using faithful stochastic proximity embedding," *IEEE Geosci. Remote Sens. Lett.*, vol. 12, no. 1, pp. 18–22, 2015.

[13] X. He and P. Niyogi, "Locality preserving projections," in *Proc. Adv. Neural Inf. Process. Syst*, vol. 16, 2003, pp. 585–591.

[14] M. M. Crawford, L. Ma, and W. Kim, "Exploring nonlinear manifold learning for classification of hyperspectral data," in *Opt. Remote Sens*, 2011, vol. 3, pp. 207–234.

[15] T. Wilson, S. Rogers, and M. Kabrisky, "Perceptual-based image fusion for hyperspectral data," *IEEE Trans. Geosci. Remote Sens.*, vol. 35, no. 4, pp. 1007–1017, 1997.

[16] M. Mignotte, "A multiresolution markovian fusion model for the color visualization of hyperspectral images," *IEEE Trans. Geosci. Remote Sens.*, vol. 48, no. 12, pp. 4236–4247, 2010.

[17] ——, "A bicriteria-optimization-approach-based dimensionality-reduction model for the color display of hyperspectral images," *IEEE Trans. Geosci. Remote Sens.*, vol. 50, no. 2, pp. 501–513, 2012.

[18] K. Kotwal and S. Chaudhuri, "Visualization of hyperspectral images using bilateral filtering," *IEEE Trans. Geosci. Remote Sens.*, vol. 48, no. 5, pp. 2308–2316, 2010.

[19] N. P. Jacobson, M. R. Gupta, and J. B. Cole, "Linear fusion of image sets for display," *IEEE Trans. Geosci. Remote Sens.*, vol. 45, no. 10, pp. 3277–3288, 2007.

[20] C. Xu, D. Tao, and C. Xu, "A survey on multi-view learning," *Neural Comput. Appl.*, vol. 23, no. 7-8, pp. 2031–2038, 2013.

[21] L. Ming and W. Shunjun, "A new image fusion algorithm based on wavelet transform," in *Proc. 5th Int. Conf. Comput. Intell. Multimedia Appl.*, 2003, pp. 154–159.

[22] T.-M. Tu, P. S. Huang, C.-L. Hung, and C.-P. Chang, "A fast intensity-hue-saturation fusion technique with spectral adjustment for ikonos imagery," *IEEE Geosci. Remote Sens. Lett.*, vol. 1, no. 4, pp. 309–312, 2004.

[23] L. Alparone, L. Wald, J. Chanussot, C. Thomas, P. Gamba, and L. M. Bruce, "Comparison of pansharpening algorithms: Outcome of the 2006

grs-s data-fusion contest," *IEEE Trans. Geosci. Remote Sens.*, vol. 45, no. 10, pp. 3012–3021, 2007.
[24] Z. Wang, D. Ziou, C. Armenakis, D. Li, and Q. Li, "A comparative analysis of image fusion methods," *IEEE Trans. Geosci. Remote Sens.*, vol. 43, no. 6, pp. 1391–1402, 2005.
[25] H. Wang and C. Glennie, "Fusion of waveform LiDAR data and hyperspectral imagery for land cover classification," *ISPRS. J. Photo. Remote Sens.*, vol. 108, pp. 1–11, 2015.
[26] M. Miltiadou, M. Warren, M. Grant, and M. Brown, "Alignment of hyperspectral imagery and full-waveform LiDAR data for visualisation and classification purposes," in *Proc. 36th Int. Symp. Remote Sens. Environ.*, May 2015, pp. 1257–1264.
[27] C. Wang and S. Mahadevan, "A general framework for manifold alignment," in *Proc. AAAI*, 2009, pp. 53–58.
[28] J. Ham, D. Lee, and L. Saul, "Semisupervised alignment of manifolds," in *Proc. 10th Int. Workshop Artif. Intell. Statist.*, 2005, pp. 120–127.
[29] Y. Qian, D. Liao, and J. Zhou, "Manifold alignment based color transfer for multiview image stitching," in *Proc. IEEE Int. Conf. Image Process.*, 2013, pp. 1341–1345.
[30] H. L. Yang and M. M. Crawford, "Manifold alignment for multitemporal hyperspectral image classification," in *Proc. IEEE Int. Geosci. Remote Sens. Symp.*, 2011, pp. 4332–4335.
[31] D. Tuia, M. Volpi, M. Trolliet, and G. Camps-Valls, "Semisupervised manifold alignment of multimodal remote sensing images," *IEEE Trans. Geosci. Remote Sens.*, vol. 52, no. 12, pp. 7708–7720, 2014.
[32] D. Liao, Y. Qian, and J. Zhou, "Visualization of hyperspectral imaging data based on manifold alignment," in *Proc. Int. Conf. Pattern Recogn.*, 2014, pp. 70–75.
[33] C. Wang and S. Mahadevan, "Manifold alignment without correspondence," in *Proc. IJCAI*, 2009, pp. 1273–1278.
[34] Y. Pei, F. Huang, F. Shi, and H. Zha, "Unsupervised image matching based on manifold alignment," *IEEE Trans. Pattern Anal. Machine Intell.*, vol. 34, no. 8, pp. 1658–1664, 2012.
[35] D. G. Lowe, "Distinctive image features from scale-invariant keypoints," *Int. J. Comput. Vis.*, vol. 60, no. 2, pp. 91–110, 2004.
[36] R. Szeliski, "Image alignment and stitching: A tutorial," *Found. Trends. Comput. Graph. Vis.*, vol. 2, no. 1, pp. 1–104, 2006.
[37] M. Brown and D. Lowe, "Automatic panoramic image stitching using invariant features," *Int. J. Comput. Vis.*, vol. 74, no. 1, pp. 59–73, 2007.
[38] M. Cui, A. Razdan, J. Hu, and P. Wonka, "Interactive hyperspectral image visualization using convex optimization," *IEEE Trans. Geosci. Remote Sens.*, vol. 47, no. 6, pp. 1673–1684, 2009.

Danping Liao received her B.E. degree in software engineering from Nankai University, China, in 2011. She is currently a Ph.D. candidate at College of Computer Science in Zhejiang University, China. She is also a visiting research assistant in the Vision and Media Lab, Simon Fraser University, Canada.

Her research interests include image processing, computer vision and machine learning.

Yuntao Qian (M'04) received the B.E. and M.E. degrees in automatic control from Xi'an Jiaotong University, Xi'an, China, in 1989 and 1992, respectively, and the Ph.D. degree in signal processing from Xidian University, Xi'an, China, in 1996.

During 1996–1998, he was a Postdoctoral Fellow with the Northwestern Polytechnical University, Xi'an, China. Since 1998, he has been with the College of Computer Science, Zhejiang University, Hangzhou, China, where he is currently a Professor in computer science. During 1999–2001, 2006, 2010, and 2013, he was a Visiting Professor at Concordia University, Hong Kong Baptist University, Carnegie Mellon University, the Canberra Research Laboratory of NICTA, and Griffith University. His current research interests include machine learning, signal and image processing, pattern recognition, and hyperspectral imaging.

Prof. Qian is an Associate Editor of the IEEE JOURNAL OF SELECTED TOPICS IN APPLIED EARTH OBSERVATIONS AND REMOTE SENSING.

Jun Zhou (M'06-SM'12) received the B.S. degree in computer science and the B.E. degree in international business from the Nanjing University of Science and Technology, Nanjing, China, in 1996 and 1998, respectively; the M.S. degree in computer science from Concordia University, Montreal, QC, Canada, in 2002; and the Ph.D. degree in computing science from the University of Alberta, Edmonton, AB, Canada, in 2006.

In June 2012, he joined the School of Information and Communication Technology, Griffith University, Nathan, Australia, where he is currently a Senior Lecturer. Prior to this appointment, he was a Research Fellow at the Research School of Computer Science, Australian National University, Canberra, Australia, and a Researcher at the Canberra Research Laboratory, NICTA, Canberra, Australia. His research interests include pattern recognition, computer vision, and spectral imaging with their applications in remote sensing and environmental informatics.

Yuan Yan Tang (F'04) received the B.S. degree in electrical and computer engineering from Chongqing University, Chongqing, China, the M.S. degree in electrical engineering from the Beijing University of Post and Telecommunications, Beijing, China, and the Ph.D. degree in computer science from Concordia University, Montreal, QC, Canada.

He is currently a Chair Professor with the Faculty of Science and Technology, University of Macau, Macau, China, and a Professor/Adjunct Professor/ Honorary Professor at several institutions including Chongqing University, Chongqing, China, Concordia University, Montreal, QC, Canada, and Hong Kong Baptist University, Hong Kong. He is the Founder and Editor-in-Chief of the International Journal of Wavelets, Multiresolution, and Information Processing and an Associate Editor of several international journals. He has published more than 400 academic papers and is the author/coauthor of over 25 monographs/books/book chapters. His current interests include wavelets, pattern recognition, and image processing. Dr. Tang is a Fellow of the International Association for Pattern Recognition (IAPR). He is the Founder and Chair of the Pattern Recognition Committee of IEEE SMC. He has served as general chair, program chair, and committee member of many international conferences. He is the Founder and Chair of the Macau Branch of IAPR.